Astron. Astrophys. 334, 289–298 (1998)

ASTRONOMY AND ASTROPHYSICS

The 09 September 1989 γ-ray flare – multi-site particle acceleration and shock-excited radio emission during quasiperpendicular and quasiparallel propagation

H. Aurass[1], **A. Hofmann**[1], **and H.-W. Urbarz**[2⋆]

[1] Astrophysikalisches Institut Potsdam, Observatorium für solare Radioastronomie und Sonnenobservatorium Einsteinturm, An der Sternwarte 16, D-14482 Potsdam, Germany

[2] Universität Tübingen, Aussenstelle Datenarchiv Weissenau, D-7980 Ravensburg, Germany

Received 6 October 1997 / Accepted 16 February 1998

Abstract. This is a case study of the location of particle acceleration sites during an impulsive flare and its subsequent coronal shock which occurred on 09 September 1989. Joint radio, hard X-ray/γ-ray, and H_α observations of the flare impulsive emissions reveal that electron and ion acceleration results from successive energy release in different magnetic structures. In this paper we attempt to identify these magnetic structures, during both the impulsive flare and the coronal shock propagation. This is done by tracing essential features identified in high time resolution radio spectral and hard X-ray/γ-ray data in radio images, and comparing the spatial information with sequences of H_α images and a static figure of the coronal magnetic field lines derived by extrapolating photospheric field measurements. During the impulsive phase signatures of energy release are found in different coronal height ranges which are magnetically connected with a small part of an underlying active region that is invaded by an expanding H_α flare ribbon. The magnetic field configuration comprises two sites at heights between $2 \cdot 10^4$ and $8 \cdot 10^4$ km above the primary highly confined flare. These sites are characterized by coronal magnetic field line systems crossing at nearly right angle. This provides for potential sites of efficient energy release and particle acceleration without demanding for extreme twist. The subsequent shock wave, revealed by type II radio burst emission, is found to propagate over large distances (~ 1 $R_\odot$) through the corona and to accelerate electrons in regions where it propagates along and across the ambient magnetic field.

Key words: Sun: radio radiation – Sun: magnetic fields – Sun: flares – Sun: X-rays, gamma-rays – shock waves

1. Introduction

In space plasmas energy is released during eruptive phenomena e.g. as streams of energetic particles, mass motions, and blast waves which can grow to shocks. Energetic particles in the solar corona can remotely be sensed in different ranges of the electromagnetic spectrum from radio waves up to γ-rays depending on their species and energy range, and on the region where they emit (cf. Miller et al. 1997; Trottet & Vilmer 1997; Vilmer & Trottet 1997 for recent reviews on particle acceleration and radiation signatures during solar flares). Much of the meter wave radio emission is due to electrons of tens of keV emitting at the local plasma frequency or its harmonic.

The comparison of these radiative signatures with extrapolated magnetic fields from photospheric measurements can provide information on possible sites of electron acceleration and supply constraints on its mechanism. This method has been developed and largely applied to the H_α signatures of energy release during flares (e.g. Démoulin et al. 1997, and references therein). In the following, we pursue the discussion of the relation between radiative signatures and magnetic field structures during the event studied by Chupp et al. (1993) and Aurass et al. (1994a), by comparing meter wave radio spectral and imaging data with field line plots obtained by extrapolating photospheric magnetographic measurements. We address two problems related with electron acceleration during flares:

1. The distribution of acceleration sites in the atmosphere during intense flares. Although typical heights of acceleration are of the order of 10^4 km above the photosphere, simultaneous acceleration above 10^5 km (Kane et al. 1992) and even above 1 $R_\odot$ (Klein et al. 1997) has been reported. In a series of comparative studies of γ/hard X-ray, optical and metric radio observations of impulsive flares, Raoult et al. (1986), Chupp et al. (1993), Trottet et al. (1993), Aurass et al. (1994a) and Trottet et al. (1994) have shown that γ-ray and radio emissions with distinctly different spectral characteristics come from different sites within a flaring active region. While these findings show indirectly that different magnetic field structures participate in the flare energy release process, explicit comparisons with magnetic field data are still rare.
2. The question where in the coronal magnetic field a large-scale shock wave excites radio emission (type II bursts - cf. Nelson and Melrose 1985, Mann 1995, Aurass 1997 for fur-

Send offprint requests to: H. Aurass

⋆ Hans Walter Urbarz passed away on 23 July 1996.

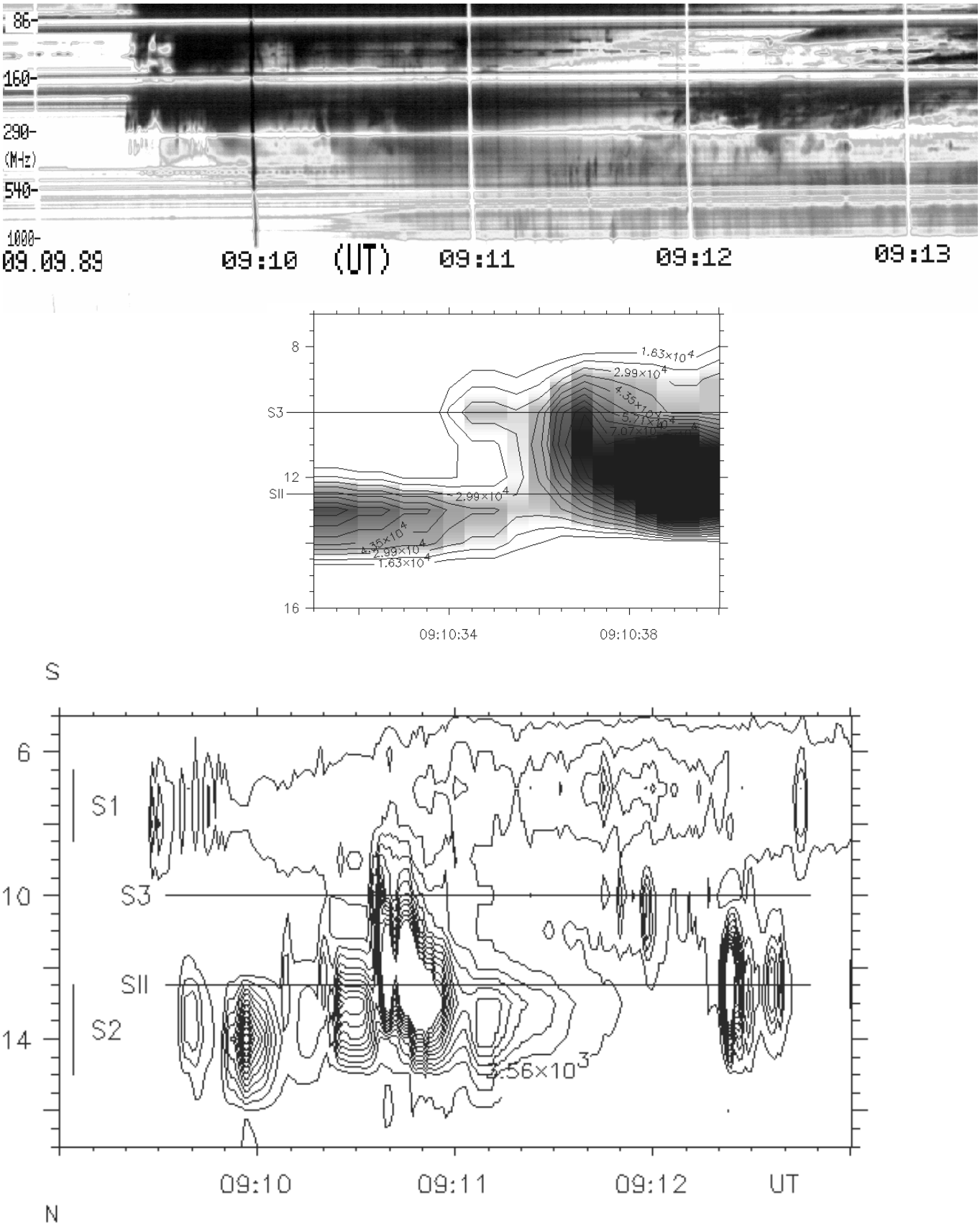

Fig. 1. Top: The Weissenau spectrum, 70-1 000 MHz. Middle and bottom: (courtesy by K.- L. Klein and G. Trottet): NRH 327 MHz isolines, one-dimensional north-south scan over the solar radio brightness. S 1 and S 2 site ranges are denoted by a bar at the left margin. S 3 is the narrowband source visible at the beginning of strong high-energy emission; S II is the site of the definitive type II onset at 327 MHz (09 : 12 : 30 UT). The middle panel gives an enlargement of the 10 seconds around the S 3 flash.

ther reference) and whether the electrons are preferentially accelerated in quasi-parallel or quasi-perpendicular regions of the shock wave.

2. Instrumention and methodology

Radio spectral observations in the 30-1 000 MHz domain were obtained by the Weissenau sweep spectrometer (e.g. Urbarz 1990). The spectra shown in this paper have been digitally scanned directly from the film record. Vertical stripes are due to irregularities in the film transport speed.

Radio imaging observations in the metric-decimetric range were obtained with the Nançay Radioheliograph (NRH) (The Radioheliograph Group 1989). The 09 September 1989 flare was recorded with the Mark IV version of the NRH which provides one-dimensional images (total intensity and circular polarization) in the east-west (EW) direction at 164 MHz and in the north-south direction (NS) at 164 MHz, 236.6 MHz, 327 MHz, 408 MHz and 435 MHz. The spatial resolution of the NS array, which is inversely proportional to the observing frequency, was 3.8 arc minutes at 164 MHz. Four images per second were recorded at each frequency. The EW array operated only at 164 MHz with a spatial resolution of 1.6 arc minutes and a time resolution of 0.02 seconds. At 164 MHz the EW and NS one-dimensional images allow for obtaining the 2-d position of the centroid of the emitting sources, projected on the solar disk. At the other frequencies, only NS images are available and the projection on the solar disk of the actual position of a given source lies along a straight line.

Magnetic field data were taken from the vector magnetograph of Einsteinturm Observatory Potsdam (Staude et al. 1991). The measurements were performed in the wings of the Fe I 5250.2 Å line. The r.m.s. noise level corresponds to about 10 G for the longitudinal and to 100 G for the transverse fields at a pixel size of 3 arcsec. Full disk magnetograph measurements from Kitt Peak Observatory have also been used. The knowledge of the full vector enables to correct the Potsdam magnetogram for spherical off-center distortions and to transform it to vertical local solar coordinates.

Basing on Seehafer (1978) we calculated three-dimensional linear force-free magnetic fields. We used the transformed vector magnetogram as well as parts of the Kitt Peak magnetogram with different spatial grid resolutions (varying between 12 and 4 arcsec) and field of view (FOV) as boundary condition. The extrapolation of the transformed data yields a spatially highly resolved field structure near the flare ribbons. On the other hand the lower resolution extrapolations based on the Kitt Peak data describe the gross field connections to the more remote surroundings. Within the smaller FOV of the Potsdam instrument the field connections obtained by extrapolating the line-of-sight data (Kitt Peak) are well comparable with those derived from the spherically corrected and transformed data. Thus we found a compromise for extracting information about the coronal magnetic field structure from the photosphere up to about 300 000 km height as necessary for a comparison with the radio imaging data obtained by the NRH at 164 MHz and higher frequencies. In order to get readable figures we have only drawn those field lines leaving the extrapolation box in a prescribed height range, or closed field lines with a turning point in a given height range, or field lines with a prescribed start and end footpoint area. The plane geometry approach of the extrapolation is justified for our purpose because the large scale magnetic field pattern nicely fits with streamer and ray pattern positions observed with the Solar Maximum Mission white light coronograph (Burkepile and St. Cyr 1993, and Burkepile, personal communication).

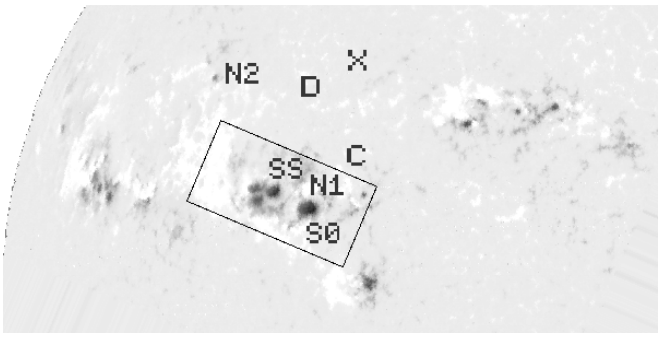

Fig. 2. The Kitt Peak magnetogram of the north-eastern part of the disk. Top is north; white: north polarity; black: south polarity. The frame gives the position of the Potsdam vector magnetogram FOV (295 x 145 arcsec). The primary flare site is in and around the north polarity N 1 which is an intrusion in south polarities SS and S 0. N 2, C and D refer to north polarity regions, remote from the primary flare site (see text). Site X is the projected onset site of the 164 MHz type II source.

3. Observations

The 09 September 1989 H_α 1B flare (GOES X 1) occurred in NOAA region 5680 (N18, E28) at 09 : 08 UT. The comparison of radio, optical and hard X-ray/gamma-ray observations of this flare has been presented in Chupp et al. (1993) and in Aurass et al. (1994a). In the following we add detailed radio spectral and photospheric magnetic field data and compare specific radio features with the extrapolated magnetic field structure.

3.1. Radio observations

Fig. 1 shows the Weissenau spectrogram (top panel) together with the isointensity contours for the one-dimensional 327 MHz NRH north-south scans (bottom panel) during the first four minutes of the event. Chupp et al. (1993) have indicated that the radio emission arises from three distinct regions (marked S 1, S 2 and S 3 in Fig. 1) which switch on sequentially in time. They also notice a type II burst at 09 : 12 : 30 UT which occurred at a position marked S II in Fig. 1, which is slightly different from S 2. A more detailed inspection of the NRH data reveals that S II is already emitting at 09 : 10 : 07. Spectral data shown in Fig. 1 indicate that the type II burst consists of patchy harmonic emission with superposed fast drift features. The fast drift bursts have a well defined low frequency cut-off and remind to spectral patterns that often precede the well expressed type II burst

lanes (Aurass et al. 1994b). At lower frequencies ($\sim$ 160 MHz) a faint lane of fundamental mode emission starts at 09 : 11 : 20 UT and drifts slowly toward lower frequencies.

The radio emission proceeds in different sources distributed over a range of 0.4 $R_\odot$ in projection at 327 MHz:

- Fast-drift (type III) bursts and continuum emission start around 09 : 09 : 30 UT in S 1 at the southern border of this range.
- S 2 switches on about 10 s later at the northern border. Its emission consists of continuum-like features with superposed fast-drift bursts (diffuse reverse drift (RS) and type III bursts). Hard X-ray emission starts together with S 2 (Chupp et al. 1993).
- A new source S II, which brightens alternately with S 2, rises between 09 : 10 and 09 : 11 UT. The emission consists of fast drift bursts, including at least one RS burst (09 : 10 : 20 UT).
- Narrow-band emission is seen from S 3 (observed at 327 MHz but not at the adjacent NRH frequencies). The middle panel in Fig. 1 shows that between 9 : 10 : 34 and 9 : 10 : 39 (during a diffuse RS burst feature in the spectrum) three distinct brightenings occur successively at S 3, between S 3 and S II and at S II. The highest γ-ray emission at $h\nu > 10$ MeV (Chupp et al. 1993) occurs together with this S 3-S II radio emission.

3.2. Magnetic field and H_α data

Fig. 2 shows the NE-part of the full-disk magnetogram from Kitt Peak Observatory (mean observing time 15 : 20 UT). The inserted black box marks the position of a Potsdam vector magnetogram of AR 5680 (07 : 37-08 : 44 UT).

The flare ribbon pattern consists of three features (Chupp et al. 1993; Aurass et al. 1994a):

- A circular two-ribbon flare configuration is centered around the north polarity intrusion (N 1) in the south polarity field (SS). The inner dotlike flare ribbon is centered above N 1, the outer circular ribbon touches the big southern spot S 0.
- A remote north polarity site C lies almost at the boundary of the Potsdam FOV.
- A remote north polarity site D[1] is far outside of the Potsdam FOV.

The sites C and D are denoted by arrows in Fig. 7 of Chupp et al. (1993). Both remote patches (C later than 09 : 10 : 11, D after 09 : 11 : 15 UT) brighten in the wings of the H_α line in association with the radio sources S II and S 3 (compare Fig. 1 and Sect. 3.1).

Fig. 3 shows the primary flare site (PS henceforth) around the north polarity intrusion N 1 in a side perspective view. We have drawn field lines of the extrapolated coronal magnetic field rooted in N 1 and in region C with turning heights below 30 000 km above the photosphere. The figure discloses that the primary flaring proceeds in very low heights. The field lines

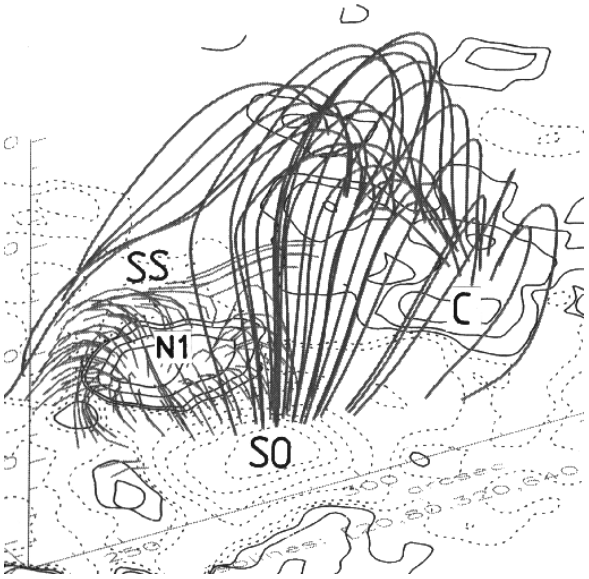

Fig. 3. Characteristic field lines of a potential field extrapolation. Perspective view, height range 0-30 000 km. The coordinate axis in the foreground is east-west-directed. The circular pattern around the N 1 intrusion and a connection SS-C is situated below 10 000 km height. The field line systems SS-C and S 0-C are inclined to each other in the top of the primary two ribbon flare site. We call this bunch of field lines the LOW system (L henceforth). Its southpolar footpoints are touched by the outer ribbon of the primary circular flare. Both systems are below an arch system S 0-N 2 shown in Fig. 4.

of the circular field arcade around N 1 - following in detail the early H_α signatures - all turn below 10 000 km height.

Tracing the surroundings of the southpolar roots of arcade field lines one finds three different field line subsets connecting this area with the northpolar site C:

- to the northwest of N 1, there is rooted a connection below 10 000 km height. This appears like a flat bridge in the background of Fig. 3.
- to the south of N 1 but northward of spot S 0.
- east- and northward of N 1.

The field lines of the two last subsets (we call them system L) converge in heights between 10 000 and 30 000 km above the region N 1. Note that these lines orthogonally cross in projection an overlying field system of larger span as becomes clear from Fig. 4.

There are given selected field line connections of the extrapolated coronal field above a larger part of the photosphere in topside perspective. Like in Fig. 3, we searched for field lines rooted around the N 1 intrusion (at PS). Again we find three field line systems relating the further surroundings of N 1 with widely spaced sites:

- to the north of N 1, there is a connection to the remote north polarity site D (turning point between 20 000 and 80 000 km height, drawn as thin field lines in Fig. 4). According to our terminology, this is field line system MD.

[1] With the present paper we correct a wrong statement about the field polarity of site D given in Aurass et al. 1994a.

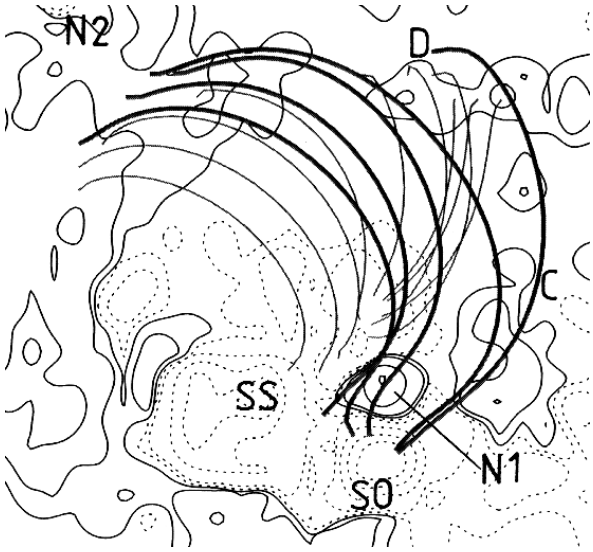

Fig. 4. Topside view of the characteristic field lines of a potential field extrapolation. North is up, east is left. Thin lines: field in the 20 000-80 000 km height range – the MEDIUM (M) system including MN and MD. Thick lines: field in the 65 000-150 000 km range – the HIGH (H) system including HN and HD.

.

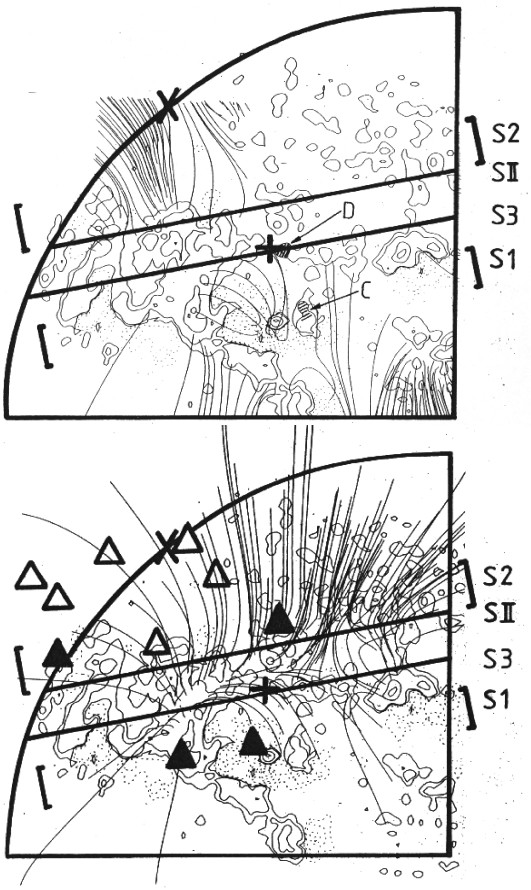

Fig. 5. Superposition of radio source positions (composite of Figs. 3b and 3c in Chupp et al. 1993) with field line patterns, seen by a terrestrial observer, in the 50 000 - 100 000 km height range (top panel) and above 280 000 km (bottom panel). Lines and bars show the source sites, marked in Fig. 1 resulting from one-dimensional NS scans at 236.6, 327, 408 and 435 MHz. The + sign gives the S 1 site, the cross the S 2 site at 164 MHz. Open and closed triangels: source sites of fast drift bursts at 164 MHz. Open triangles denote those fast drift burst sites passed by the 164 MHz type II burst source later in the event.

– to the east and northeast of N 1, the south polarity region SS is connected with region N 2. Magnetic connections exist in the height ranges 20 000-80 000 km (thin field lines, MN) and 65 000-150 000 km (thick field lines, HN). Note the connectivity transition from C to N 2 with distance from N 1, and with height, respectively; compare Figs. 3 and 4.
– The space between N 1 and the spot S 0 is in larger heights interconnected with the remote site D (thick field lines, system HD).

Fig. 4 allows an independent check of the given presentation of the coronal magnetic field. There is a field line connecting spot S 0 with remote site D. The field line passes in projection above the remote site C. The correctness of this result of the potential field approximation is confirmed by a detail in the H_α images of Chupp et al. (1993), Fig. 7. In the blue wing panels (9 : 10 : 00 to 9 : 12 : 09 UT) a surge ejection out of S 0 is seen pointing towards C and later (past 09 : 14 : 32 UT[2]) also to D but in the red wing.

Comparing Figs. 3 and 4 we summarize that there are several regions between the photosphere and about 80 000 km height in which initially independent field line systems orthogonally cross each other. Volumes enclosing ranges of superposed and quasiorthogonal field lines are potential reconnection sites (e.g. Priest 1984). If the primary flaring circular arcade starts rising (observationally confirmed by expansion of the circular flare ribbon, see Fig. 7 in Chupp et al. 1993) it would touch and interact with overlying systems and / or excite those field line systems which are rooted with one footpoint in the surroundings of N 1. This can lead to the sequential activation of the identified potential reconnection sites in different height ranges.

3.3. Impulsive phase radio sources and the field data

With reference to Fig. 1, the Fig. 5 (top panel) shows the location of radio sources S 1 - S 3 and S II superposed on field lines turning or leaving the extrapolation box between 50 000 and 100 000 km above the photosphere. Fig. 5 (bottom panel) is a superposition of the same sources with a field line map for heights above 280 000 km. This panel contains only open field lines (arched lines leave the box at its front side!). In examining Fig. 5 we note:

– The projections of fast drift burst source sites (around both S 1 and S 2)[3] fall on open field lines leaving the northeastern site N 2 which are well seen in the potential field ex-

[2] G. Trottet gave us access to the original plates for this figure enclosing some more panels than shown in Chupp et al. (1993).

[3] The 2-d positions can only be determined at 164 MHz!

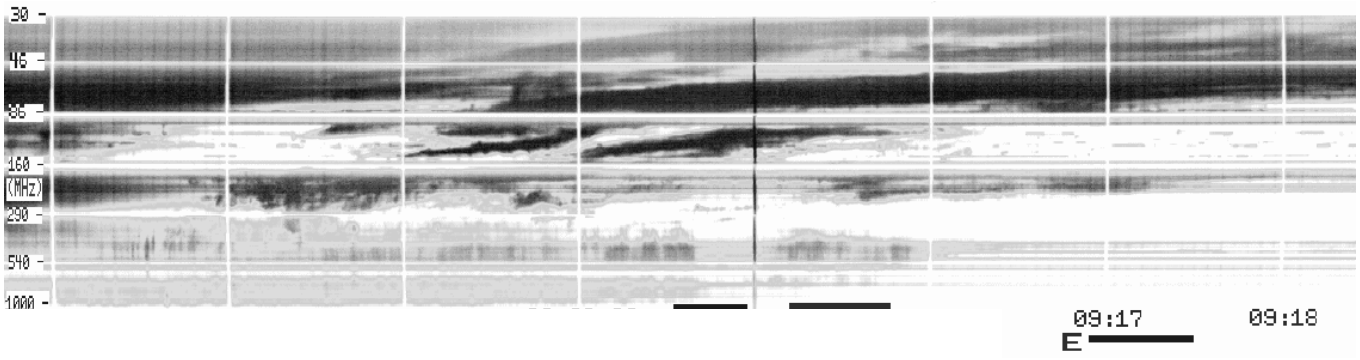

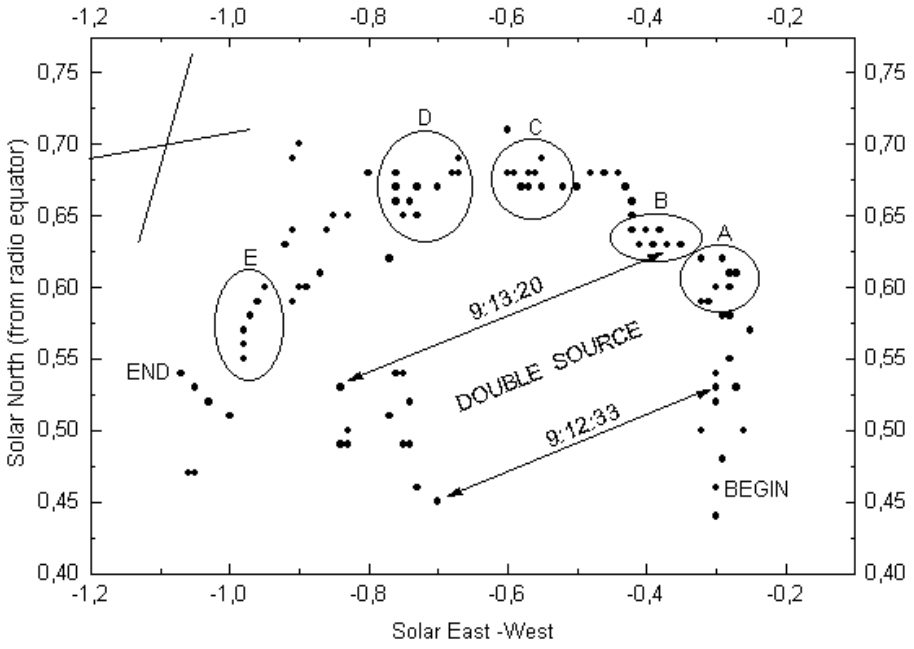

Fig. 6. Top: The Weissenau type II burst radio spectrum on 09 September 1989. Bottom: The projected positions of the 164 MHz radio type II burst observed at different times between 09 : 12 and 09 : 15 UT (dots, courtesy by G. Trottet and K.- L. Klein). Capital letters refer to time intervals given in the top. The cross in the upper left is a representative half-power dimension of the 164 MHz source.

trapolation at heights above 280 000 km (triangles in Fig. 5, bottom).

- At high frequencies, the source S 1 is situated above the circular H_α flare ribbons around the N 1 spot. At 164 MHz (+ sign in Fig. 5) the source is shifted northward indicating that S 1 is a continuum emission due to confined energetic electrons in the closed loop configurations MN and HN. This is supported by the 60-80 % right hand circular polarization of the broad band source (o-mode emission according to the leading spot hypothesis, Krüger 1972).
- We suggest that the positions of the S II and S 3 sources result from contacts between systems L (Fig. 3) with HN (Fig. 4) and MD with HN, HD (Fig. 4).
- S 2 emission starts at least 50 s before S 3 (see Fig. 1). In Sect. 3.2 we found that in the surroundings of PS there are field line footpoints leading to the region N 2. Further, we found a potential reconnection site between systems L and HN. If at this site reconnection starts the remote site C will brighten. Further, accelerated particles can find their way toward N 2. But it is not clear how type III electron beams driving the S 2 sources at low frequencies (triangles in Fig. 5 bottom) are accelerated near to the open field line footpoints rooted in N 2.

Summarizing we claim that the derived magnetic connectivity can explain the energy flow causing H_α emission at the remote sites C and D. Further it helps to enlighten the widespread distribution of impulsive radio sources in the active region atmosphere without yielding a completely satisfying picture.

3.4. The type II burst and the field data

Generally, the slowly drifting lanes of meter wave type II bursts are visible at a given frequency above 100 MHz during about 1 - 2 minutes, possibly also less if one traces a well defined spectral subfeature (e.g. a given split band). At 164 MHz, the NRH observed most often a source at a fixed position or a source moving over a small fraction of the solar radius (K.- L. Klein, pers. com.). In the present event the situation is quite different. The type II burst shown in Fig. 6 (top) has a multiple lane structure. Fig. 6 (bottom) gives a path - time curve on the disk for the shock-driven 164 MHz radio source. Between 9 : 12 and 9 : 15 UT one finds at least three different pairs of fundamental - harmonic lanes between 300 and 30 MHz. The dots in Fig. 6

Table 1. Spectral and imaging characteristics of the moving disturbance around the NRH imaging frequency (164 MHz), see also Fig. 6

Time (9 : min : s UT)	Spectral Effect	Imaging Information	Ref. to Fig.
from 11 : 20	faint f - mode lane at $<$ 160 MHz; above dm-like patches and drift bursts	source visible in low field cone below converging ray dm sources tend from S 3 to S II	1, 6, 7, 8
12 : 30	At 130 MHz clear f - mode lane		
12 : 30	* * * * * * * * * * * * * * * * * *	** two sources are visible **	6
from 12 : 45	clear but faint lane $<$ 160 MHz	source consists of 2 parallel moving	
from 13 : 00	strong lane $<$ 160 MHz	subsources	
until 13 : 10 - 15	end of the dm-like effects $>$ 160 MHz positive lane drift until 09 : 13 : 40 - 50	distance in projection: 0.5 $R_\odot$	A in 6
13 : 20	* * * * * * * * * * * * * * * * * *	** the SE subsource decays **	B in 6
13 : 35 - 14 : 05	diffuse type IIIs start from the lanes and are visible till 50 MHz.	the main type II source leaves the low field cone below the converging ray	8
from 13 : 45	new lane at $<$ 160 MHz		
until 14 : 20	narrow band lane reaches 160 MHz	most westward subsource appears	C in 6, 8
15 : 10	vis. until 09 : 15 : 10 also at f $<$ 160 MHz	most westward subsource disappears	
15 : 20 - 16 : 30	splitted lanes at $>$ 160 MHz		D in 6
16 : 40 - 17 : 15	again splitted lanes at $>$ 160 MHz		E in 6

show the positions of the type II emitting source centroid during fixed time intervals.

In comparing both panels of Fig. 6 (see also Table 1) we note that the radio sources are moving during each spectral lane and that the sources of subsequent lanes are progressively shifted eastward. This is observed over a total distance of $\sim$ 1 $R_\odot$ between the time intervals A (the high frequency edge of the first lane that attains 164 MHz) and E (the low frequency edge of the last lane attaining 164 MHz).

The type II source sometimes displays a continuous movement, while stopping at a given position on other occasions. Between 09 : 12 : 33 and 09 : 13 : 20 UT two subsources appear with a projected distance of about 0.5 $R_\odot$. The systematic shift of the radio source suggests that the different spectral lanes occur when a given disturbance encounters different coronal plasma structures. The apparant speed of the spatial displacement along the trace shown in Fig. 6 is about 2 000 km s^{-1}. Thus we can track the radio source driven by a flare-induced super-Alfvénic disturbance during its contact with the 82 MHz plasma level (according to the spectral data 164 MHz emission is the harmonic mode) for more than five minutes. Note by comparison with the spectrogram that we see at the NRH observing frequency a more or less radially escaping feature of the shock front in the first minute (till $\sim$ 09 : 13 UT), only. Later the main type II lanes appear at lower frequencies. Shock signatures at 164 MHz are now from the outer rim of the disturbance during its more or less azimuthal propagation along the 82 MHz plasma level. The height modulation of this level seems to be very strong so that the same (semispheric) disturbance can sequentially brighten at different sites in different altitudes. This leads to the multilane pattern in the spectral diagram.

AR 5680 belongs to an east-west extended belt of active regions and is situated at a north-south boundary of the global background field. To the northwest of the region, there extends an area of weak fields with northern polarity. This situation is reflected by the potential field extrapolation, height range between 100 000 and 200 000 km given in Fig. 7 (left panel). Open field lines rooted in faint northern background fields form a belt which is open mainly toward AR 5680. On the other hand, east of AR 5680 there are open field lines rooted in northern polarity belonging to the eastern part of the region and to its followers. So, in the given height range, the flaring active region is more or less azimuthally confined by open field lines extending to large coronal heights. This is confirmed by two bright rays in the SMM coronograph data which reveal the continuation of the two groups of open field lines to heights above 2 $R_\odot$ (J. Burkepile, pers. com.). The open field lines converge at heights above 280 000 km thus forming a ray - not a streamer, because all the footpoints are rooted in the same polarity !

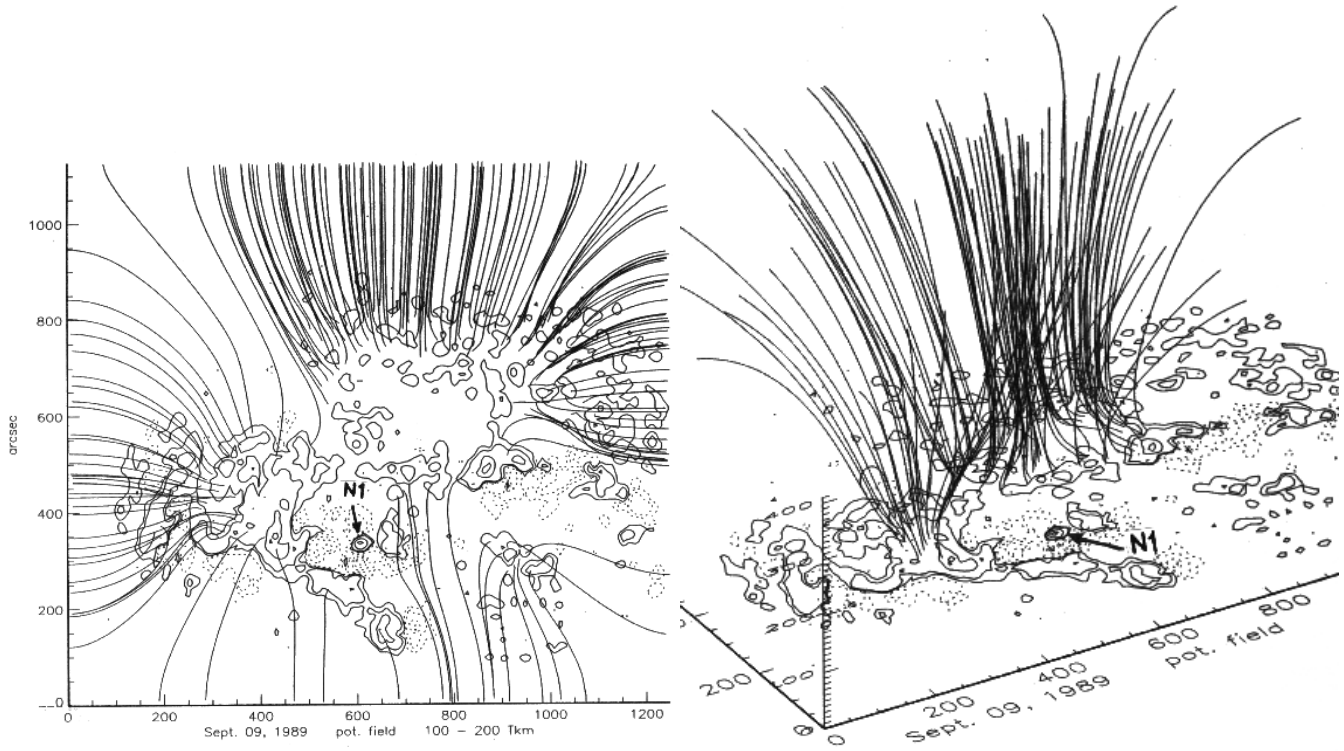

Fig. 7. Potential field extrapolation of a large area around NOAA 5680. An arrow points to the N 1 intrusion. Left panel: terrestrial observer's view of field lines in the 100 000-200 000 km height range. Right: perspective representation of the field structure above 280 000 km height (foreground coordinate axis east - west directed). Open field lines rooted in north polarity converge thus forming a conic ray overlying the low field area.

Fig. 7 (right panel) displays this situation in a perspective view (it is the same field line pattern as in Fig. 5, bottom). To the northwest of AR 5680, there is a low field region with field lines converging with increasing height. Fig. 8 presents a superposition of the complete 164 MHz type II burst trace (thick black line) onto the set of field lines shown in Fig.7 (right panel) as seen from earth. The figure suggests that inside the ray there is a region of low Alfvén speed within which the disturbance is focused by refraction (remind also the field line wall around this area presented in Fig. 7 left panel). The disturbance starts growing to a shock wave and accelerating electrons during its upward propagation in the ray. In this time interval the disturbance moves more or less parallel along the magnetic field lines.

Between 09 : 13 : 35 and 09 : 14 : 05 UT the shock-driven radio source bends out of the conic field pattern of the ray in eastward direction. Remarkably, simultaneously low frequency strong drift bursts appear in the spectrum (see Fig. 6, 9 : 13 : 40 - 9 : 14 UT between 120 and 50 MHz). Since the spectrum does not show drift burst signatures arriving from higher frequencies, these drift bursts seem to be excited by shock-accelerated electrons escaping along the field lines of the ray structure. The appearance of these specific fast drift bursts during the time interval in which the shock front leaves the open field lines forming the ray is an independent argument for the good fit between the computed field line pattern and the observed shock wave trace.

In the same time interval a new lane appears. Its high frequency edge is observed at 164 MHz by the NRH. This pattern dominates the spectrum until 9 : 14 : 20 UT. In this time, a new (the farthest westward situated) sub-branch of the type II burst becomes visible which has not been drawn in the path - time diagram (Fig. 6). It starts in projection near to the type II burst onset region but drifts in south-east direction, seemingly perpendicular to well visible northwestward arched open field lines. After leaving the low-field cone the dominant burst source moves - at least in projection - perpendicular to the background field lines, too. During double source emission the eastern branch (Fig. 6) seems to slide along a bundle of open field lines. The burst trace of the late part of the type II disturbance coincides in projection with the intersection of the observed plasma level by earlier appearing type III sources (open triangles in Fig. 5 bottom). The coincidence also confirms our statement about quasiperpendicular propagation of the shock in the late part and about quasiparallel propagation during the excitation of the eastward branch of the double source. In this case, the corresponding field line bundle was also illuminated before by an independent type III burst (see Fig. 5 bottom).

We conclude that the analyzed event yields some evidence of shock-driven electron acceleration unlimited by the angle between the shock normal and the magnetic field direction.

4. Summary and conclusions

In this case study we search for particle acceleration sites in the coronal atmosphere around a comparatively simple active re-

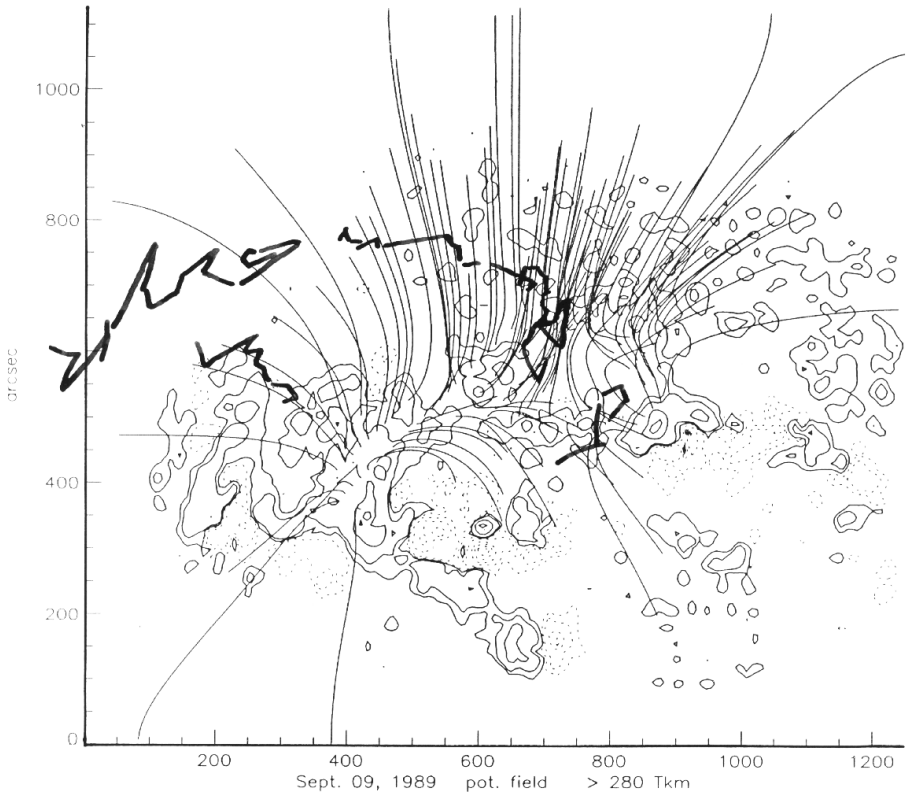

Fig. 8. The complete 164 MHz type II burst source path (bold line) superposed to the observers perspective of the potential field extrapolation at heights above 280 000 km. Both axis are scaled in arcseconds.

gion. To this end, we present a comparison of radio and optical flare signatures with the field line topology of the coronal magnetic field on different spatial scales. The coronal magnetic field line pattern has been derived by combining the results of force-free and potential field extrapolations of photospheric magnetograms. Thereby we assume in accordance with the generally accepted experience that the photospheric field is not basically changed by the flare. Further we take the calculated field line pattern as characteristic for the preflare situation and identify in this configuration probable energy release sites near to the projected sites of flare related radio sources. The term "probable energy release site" is used for a volume with a field geometry preferable for the onset of magnetic reconnection.

The observations bear evidence on the successive evolution of energy release sites to higher altitudes. The flare starts in a circular two-ribbon configuration confined to altitudes below 10 000 km. The outer flare ribbon invades during its expansion an area which is magnetically complex connected with several more or less remote sites in and in the surroundings of the active region. Thereby the contacted field systems become activated (spread of the flare energy release according to Machado et al. 1988).

During the main radio and γ-ray event we can identify beside and above the compact PS at least two distinct regions in different height levels of the corona. In these regions magnetic energy can be released by reconnection if the derived static field configuration is disturbed. The disturbance is the rise of the PS field system. One distinct region appears between 20 000 and 30 000 km, the second distinct region is situated in the interval 60 000 to 80 000 km. In the distinct regions almost orthogonal field line systems approach each other. The potential for high magnetic energy release is inherent in the given field topology and does not demand for additional and extreme twisting. Note that for our analysis it was sufficient to consider deviations from the potential field only in a very restricted cube of the flaring atmosphere with a scale of several thousands of kilometers. This coincides with the main result of Hagyard et al. (1990) who could not find differences in the shear of the photospheric magnetic field in comparing non-γ-ray and γ-ray flares.

The delayed action of distributed energy release sites in a height range of 80 000 km and in a time interval of about 2 min naturally explains the sudden increase of interacting particles by an order of magnitude during the event reported by Chupp et al. (1993). The presented analysis confirms the general statement by these authors that particle acceleration and transport take place in a complex magnetic field geometry. Further it exemplifies high coronal particle acceleration sites during γ-ray flares already in the impulsive flare phase as described by Akimov et al. (1996) for the late flare phase.

The discussion of the impulsive phase phenomena has shown that the first radio signature of a coronal shock wave is exited in close temporal and spatial interconnection with the main energy release event. The present event gives the opportunity to trace this disturbance due to its type II burst harmonic mode emission seen at 164 MHz during 5 minutes on its path through the corona. The radio emission from the extended coronal shock wave starts far outside the active region at a site of extremely low local magnetic field. This is below a stable ray structure visible in coronographic data up to heights larger than 2 $R_\odot$. The low field strength argues for emission from a region

of low Alfvén speed, consistent with the refraction of a magnetohydrodynamic wave (Uchida 1974). Radio emission from the shock occurs subsequently in sources which at different times of the event move along or across ambient magnetic field lines.

We consider this as evidence that the shock wave accelerates electrons both in regions where it propagates along the magnetic field (quasi-parallel regime) and in regions where it is nearly perpendicular to the undisturbed field. This is consistent with predictions of the electron acceleration model by Mann and Claßen (1995). It is remarkable that at the time when the radio emitting shock at the 82 MHz plasma level leaves the cone formed at the bottom of the ray structure, one sees diffuse strong type III bursts extending to low frequencies. It seems that the corresponding electron beams which escape along the ray field lines have been directly accelerated by the shock wave (see also Mann et al. 1997).

We finally mention that with the knowledge of the field structure and the sites of the different radio sources it is quite natural in the discussed event that at a given observing frequency type III burst and type II burst sources can appear at the same site. It is obvious from Fig. 8 that this coincidence is not an argument for quasiparallel shock propagation, as used for instance by Dulk et al. (1971).

Acknowledgements. We thank G. Trottet and K.-L. Klein (Paris - Meudon Observatory) for the supply of the isoline plots shown in Fig. 1 and for preparing the data shown in Fig. 6, bottom. Their critical and careful reading of the manuscript and many common discussions have essentially improved the presentation of our results. The authors are highly indebted to the staff of the Nançay and Weissenau Radio Observatories. NSO / Kitt Peak data used here are produced cooperatively by NSF/NOAO, NASA/GSFC and NOAA/SEL. H.A. is grateful to J. Burkepile for the kind presentation of coronograph data. Further he thanks G. Mann, A. Klassen and H.-T. Claßen for stimulating discussions. The authors thank H.R. Detlefs, K. Arlt, G. Bartling and P. Hackenberg for software support, Mr. J.-P. Riese (Dieburg) for his support and advice in scanning film data records, and Mrs. Schewe and Lehmann for help in preparing the drawings.

References

Akimov, V.V., Ambrož, P., Belov, A.V. and 10 coauthors, 1996, Sol. Phys. 166, 107

Aurass, H., 1997, in Coronal Physics from Radio and Space Observations, Trottet, G. (ed.), Lecture Notes in Physics 483, Springer, Berlin, p. 135

Aurass, H., Hofmann, A., Rieger, E., 1994a, ApJS 90, 707

Aurass, H., Magun, A., Mann, G., 1994b, Space Sci. Rev. 68, 211

Aschwanden, M.J., Benz, A.O., 1995, ApJ 438, 997

Burkepile J.T., St. Cyr O.C., 1993, NCAR/TN 369+STR, HAO, Boulder, U.S.A.

Chupp, E.L., 1996, in High Energy Solar Physics, Ramaty, R., Mandzhavidze, N., Xin-Min Hua (eds.), AIP Conference Proc. 374, AIP Press, Woodbury, New York, p. 3

Chupp, E.L., Trottet, G., Marschhäuser, H., Pick, M., Soru - Escaut, I., Rieger, E., Dunphy, P.P., 1993, A&A 275, 602.

Démoulin, P., Bagalá, L.G., Mandrini, C.H., Hénoux, J.C., Rovira, M.G., 1997, A&A 325, 305.

Dulk, G.A., Altschuler, M.D., Smerd, S.F., 1971, Astrophys. Letters 8, 235

Hagyard, M.J., Venkatakrishnan, P., Smith Jr., J.B., 1990, ApJ Suppl. 73, 159

Kane, S.R., Mc Tiernan, J., Loran, J., Fenimore, E.E., Klebesadel, R.W., Laros, J.G., 1992, ApJ 390, 687

Klein, K.-L., Aurass, H., Soru-Escaut, I., Kalman, B., 1997, A&A 320, 612; Erratum with the correctly printed figures: A&A 322, 1027

Krüger, A., 1972, Physics of Solar Continuum Radio Bursts, Akademie - Verlag, Berlin

Machado, M.E., Xiao, Y.C., Wu, S.T., Prokakis, T, Dialetis, D., 1988, ApJ 326, 425

Mann, G., 1995, in Coronal Magnetic Energy Release, Benz, A.O. and Krüger, A. (eds.), Lecture Notes in Physics 444, Springer, Berlin, p. 183

Mann, G., Claßen, H.T., 1995, A&A 304, 576

Mann, G., Aurass, H., Claßen, H.T., Klassen, A., Dröge, W., Kunow, H., 1997, in ESA SP-404, 543

Miller, J.A., Cargill, P.J., Emslie, G.A., Holman, G.D., Dennis, B.R., LaRosa, T.N., Winglee, R.M., Benka, S.G., Tsuneta, S., 1997, JGR, 102, 14631

Nelson, G.J., Melrose, D.B., 1985, in Dulk, G.A., McLean, D.J. (eds.), Solar Radio Physics, Cambridge Univ. Press, Cambridge, p. 333

Priest, E.R., 1984, Solar Magnetohydrodynamics, Reidel, Dordrecht

Raoult, A., Pick, M., Dennis, B.R., Kane, S.R., 1986, ApJ 299, 1027

Seehafer, N.: 1978, Sol. Phys. 58, 215

Staude, J., Hofmann, A., and Bachmann, G., 1991, in L. November(ed.), Solar Polarimetry, Sunspot, New Mexico, p. 49

The Radioheliograph Group 1989, Solar Phys., 120, 193

Trottet, G., Vilmer, N., Barat, C., Dezalay, J.-P., Talon, R., Sunyaev, R., Terekhov, O., Kuznetsov, A., 1993, Adv. Space Res., 13, 285

Trottet, G., Chupp, E.L., Marschhäuser, H., Pick, M., Soru-Escaut, I., Rieger, E., Dunphy, P.P., 1994, A&A, 288, 647

Trottet, G., Vilmer, N., 1997, in Solar and Heliospheric Plasma Physics, Simnett, G.M., Alissandrakis, C.E. & Vlahos, L. (eds.), Lecture Notes in Physics 489, 219

Uchida, T., 1974, Solar Phys. 39, 431

Urbarz, H.- W., 1990, UAG Report 98, National Geophysical Data Center, Boulder, U.S.A.

Vilmer, N. Trottet, G., 1997, in Coronal Physics from Radio and Space Observations, Trottet, G. (ed.), Lecture Notes in Physics, 483, 28